

# Computer-Guided Design, Synthesis, and Biological Evaluation of Quinoxalinebisarylureas as FLT3 Inhibitors

Stefan Göring, Dennis Bensinger, Eva C. Naumann, and Boris Schmidt\*<sup>[a]</sup>

Activating mutations of FMS-like tyrosine kinase 3 (FLT3) are present in ~30% of patients with acute myeloid leukemia (AML) and are associated with poor prognosis. Point mutations in the tyrosine kinase domain (TKD) are observed as primary mutations or are acquired as secondary mutations in FLT3 with internal tandem duplications (ITDs) after treatment with tyrosine kinase inhibitors (TKIs). Although dozens of potent inhibitors against FLT3 ITD have been reported, activating TKD point mutations, especially at residues F691 and D835, remain the leading cause for therapy resistance, highlighting the consis-

tent need for new potent inhibitors. Herein we report the identification and characterization of novel quinoxaline-based FLT3 inhibitors. We used the pharmacophore features of diverse known inhibitors as a starting point for a new optimization algorithm for type II TKIs, starting from an in silico library pharmacophore search and induced-fit docking in the known FLT3 structure. This led to the design of a set of diverse quinoxalinebisarylureas, which were profiled in an FLT3 kinase activity assay. The most promising compounds were further evaluated in a zebrafish embryo phenotype assay.

## Introduction

Acute myeloid leukemia (AML) is a malignant disorder of the hematopoietic system characterized by uncontrolled proliferation of cells inside the bone marrow.<sup>[1]</sup> The five-year survival rate for patients under 60 years old is only 40%.<sup>[2]</sup> FMS-like tyrosine kinase 3 (FLT3) is a class III receptor tyrosine kinase including FMS, c-KIT and two genes encoding platelet-derived growth factor receptors  $\alpha$  and  $\beta$ .<sup>[3]</sup> It is the most common mutated gene in AML and has been demonstrated to play a crucial role in the development and growth of hematopoietic and non-hematopoietic cells.<sup>[4]</sup> FLT3 is composed of an N-terminal extracellular ligand binding domain with five immunoglobulin-like motifs, a transmembrane domain followed by an intracellular juxtamembrane domain, and a C-terminal tyrosine kinase domain.<sup>[5]</sup> The native ligand for FLT3 (FL) was cloned in 1993.<sup>[6]</sup> It is a type I transmembrane protein and is expressed in most tissues including hematopoietic organs (spleen and bone marrow), prostate, ovary, kidney, lung, heart, and placenta.<sup>[7]</sup> After binding of FL, the membrane-bound FLT3 undergoes a rapid conformational change including homodimerization and exposure of phosphoryl acceptor sites in the tyrosine kinase domain. This activates multiple downstream signaling pathways.<sup>[7a,8]</sup>

Two classes of activating FLT3 mutations have been identified and are present in ~30% of all AML cases. FLT3 internal tandem duplications (ITDs) occur in the juxtamembrane domain and were identified in ~23% of all AML patients.<sup>[9]</sup>

Point mutations at residues D835 or I836 in the activation loop of FLT3 are less frequent and were found in ~7% of AML cases.<sup>[2,7b,10]</sup> It was confirmed that both types of mutations constitutively activate the tyrosine kinase activity.<sup>[11]</sup>

Smith et al. first described the appearance of drug-resistant kinase mutations in FLT3 ITD-positive AML patients relapsing after treatment with quizartinib (**AC220**).<sup>[12]</sup> They found mutations at the gatekeeper (F691L) and within the activation loop (D835Y, D835V, Y842C, Y842H) conferring high degrees of in vitro quizartinib resistance.

Because of the high frequency of drug-resistant AML, there is an unmet demand for potent and selective FLT3 inhibitors.<sup>[5,7b,8,13]</sup> Quinoxalines **AG1295** and **AG1296** were the first inhibitors developed for FLT3, exhibiting an  $I+C_{50}$  value of ~1  $\mu\text{M}$  (Figure 1).<sup>[14]</sup> Consecutively, several small-molecule FLT3 inhibitors, including quizartinib (**AC220**), sorafenib (**BAY-43-9006**), sunitinib (**SU-11248**), and midostaurin (**PKC412**), have been discovered; these were evaluated in vitro and in vivo and have entered late-stage clinical trials (Figure 1).<sup>[8,14b,15]</sup> In particular, the bisarylurea **AC220** was identified and evaluated as a uniquely potent and selective FLT3 inhibitor by Chao et al. in 2009.<sup>[16]</sup> Despite considerable research efforts in academic and industrial groups, no FLT3-targeting drug has yet been approved for the treatment of FLT3-mutant AML.

## Optimization strategy

The quinoxaline scaffold can undergo alternating donor-acceptor interactions with the gatekeeper + 1/gatekeeper + 3 residues in the hinge region of the kinase domain. This binding mode has been confirmed by crystallographic observations for other kinases (Figure 2a). Docking of **AG1295** in the FLT3 hinge region explains that the observed high ligand efficiency

[a] S. Göring,<sup>†</sup> D. Bensinger,<sup>†</sup> Dr. E. C. Naumann, Prof. Dr. B. Schmidt Clemens Schöpf—Institute of Organic Chemistry & Biochemistry Technische Universität Darmstadt, 64287 Darmstadt (Germany) E-mail: schmidt\_boris@t-online.de

[†] These authors contributed equally to this work.

Supporting information for this article is available on the WWW under <http://dx.doi.org/10.1002/cmdc.201402477>.

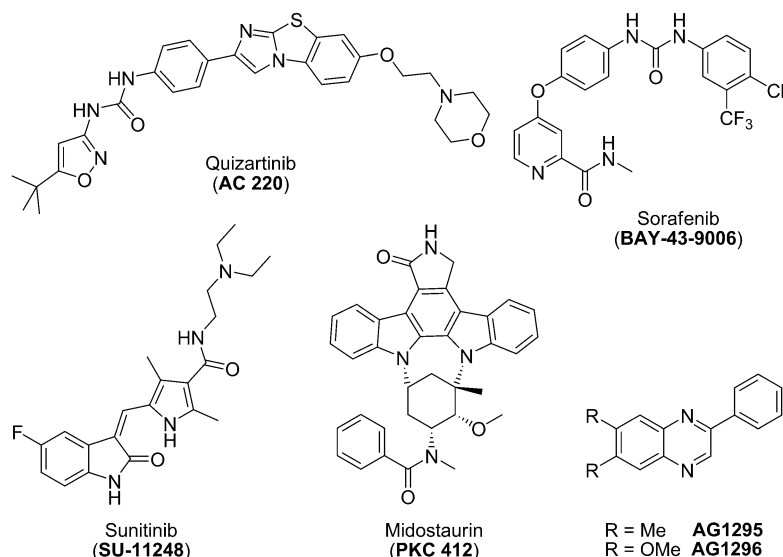


Figure 1. Selected structures of known FLT3 inhibitors.<sup>[14–15]</sup>

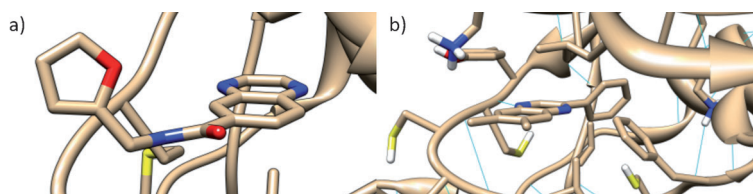


Figure 2. a) Structure of quinoxaline-based inhibitor in CHK2 (PDB ID: 4BDC) and b) result of the docking study of AG1295 in the active site of FLT3 reveals donor–acceptor interactions with the hinge region.

is due to hydrogen bonding to the hinge backbone and  $\pi$ – $\pi$  interactions with the gatekeeper F691 or F830 (Figure 2b). Substitution at the 4'-phenyl position enables interactions with the DFG motif by a tethered group, which may lead to type II inhibition. The occupation of the regulatory domain pocket by aromatic groups is frequently observed for TKIs. Due to the ubiquitous occurrence of bisarylureas connected to a hinge binding scaffold, we were interested in a general pharmacophore model for FLT3 type II TKIs binding to a kinase in a DFG<sub>out</sub>/JM<sub>out</sub> conformation. This can be observed by the co-crystallized sorafenib–VEGFR2 structure (PDB ID: 4ASD), in which the urea motif binds in the hydrophobic back pocket followed by a heterocyclic hinge binding motif.<sup>[17]</sup> This model was adapted and subsequently used to filter an in silico library of bisarylureas created by the combination of hypothetical precursor molecules with amines from our in-house chemical database (Figure 3).

A ligand-based pharmacophore represents the essential interactions of a ligand with a receptor. We used a freely accessible online database of 1675 FLT3 inhibitors with corresponding in vitro pharmacology listed.<sup>[26]</sup> For this study, eight highly potent inhibitors were selected a) because their binding mode has been solved crystallographically for other kinases or b) they are likely to exert type II inhibition and also contain

the bisarylurea binding motif (Figure 4). From this database 136 molecules with an IC<sub>50</sub> or K<sub>i</sub> value of > 1000 nM were selected at random. They were considered inactive for the preparation of the pharmacophore model.

A total of 425 pharmacophore hypotheses were generated and sorted by ascending *p* value. The accuracy of active compounds (Acc<sub>1</sub>) or inactive compounds (Acc<sub>0</sub>) is the ratio  $m_1/N_1$  and  $m_0/N_0$ , respectively, for which *N* is the total number of molecules and *m* is the number of molecules that fit the model (actives) or do not fit in the model (inactives). For Acc<sub>1</sub> = 1, all active molecules were taken into account, whereas with Acc<sub>0</sub> = 1 no

inactive molecule fit the pharmacophore hypothesis. The statistical significance of these accuracy values was determined using the  $\chi^2$ -derived *p* value. This is the base-10 logarithm of the probability of  $\chi^2$  that the accuracy results Acc<sub>1</sub> and Acc<sub>0</sub> were achieved by chance only. Lower *p* values indicate higher significance of the accuracy. The generated pharmacophores A–D contain a donor projection, acceptor projection,  $\pi$ -ring projections, and aromatic rings (Table 1). In all structures, the donor groups (NH) of the urea motif were considered as a projection, but

Table 1. Generated pharmacophore hypothesis with lowest *p* values.<sup>[a]</sup>

Entry	Pharmacophore	Acc	<i>p</i> value	Acc <sub>1</sub>	Acc <sub>0</sub>
A		0.9931	–26.2	0.875	1.0000
B		0.9861	–22.6	0.875	0.9926
C		0.9861	–22.6	0.875	0.9926
D		0.9792	–21.3	1.000	0.9779

[a] Acc indicates the overall accuracy of active (Acc<sub>1</sub>) and inactive (Acc<sub>0</sub>) compounds covered by the pharmacophore; *p* value indicates statistical significance. Generated pharmacophores consist of donor (purple), acceptor (cyan), and aromatic ring (orange) projections.

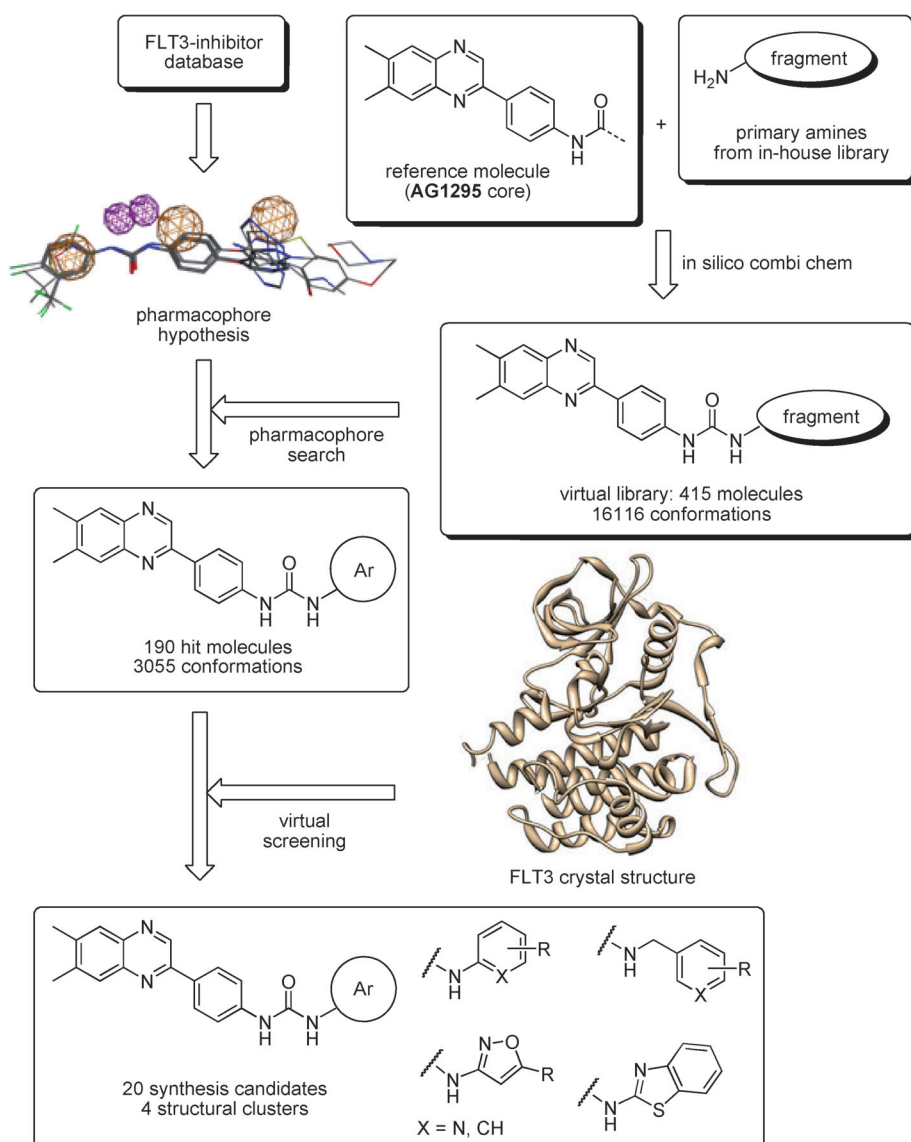


**Figure 3.** Flowchart for the optimization of quinoxaline-based TKIs starting from AG1295 using pharmacophore elucidation, pharmacophore search, and molecular docking.

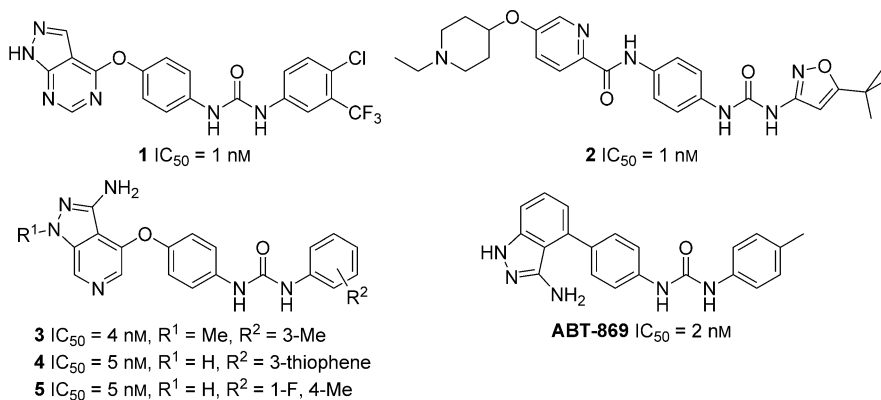


**Figure 4.** Active set of inhibitors in addition to TKIs in clinical trials (sorafenib, quizartinib) to generate pharmacophore hypothesis.

not the carbonyl acceptor. By using the pharmacophore search for various scaffolds the generated hypotheses can be superior to a single scaffold, as potential interactions can be covered more accurately. In pharmacophore hypothesis **A** each of the connecting phenyl rings as well as the various head groups are recognized, which is not the case in **B–D**. The terminal phenyl ring of the bisarylurea motif is covered by an aromatic ring center (**A**) or a projection (**B–D**) with high superposition of all molecular scaffolds. All models show a high exclusion of nearly all inactive molecules ( $Acc_0 \sim 1$ ) and include, except for the quizartinib derivative **2**, the entire set of active molecules.

The pharmacophore-based method offers a rapid assessment of many molecules using simple parameters. However, information on potential interactions between ligand and receptor and the assessment of the size of a binding pocket requires docking methods. Unfortunately, just two crystal structures are available for FLT3. In 2004, Griffith et al. described the structure of the cytosolic kinase domain, but neither in complex with an inhibitor nor ADP.<sup>[18]</sup> Due to the position of the juxtamembrane domain and the activation loop, these are in the autophosphorylated, inactive conformation (PDB ID: 1RJB). The structure of the immunoglobulin-like domains in complex with the FLT3 ligand was reported in 2012 by Verstraete et al. (PDB IDs: 3QS7, 3QS9).<sup>[19]</sup> In the next step, hits from the pharmacophore search were rated by an induced-fit docking in the kinase structure of FLT3 to assess binding geometry and potential ligand–receptor interactions.

Subsequently, sterically demanding amine fragments (bicyclics, bulky side groups, etc.) were removed, as placement in

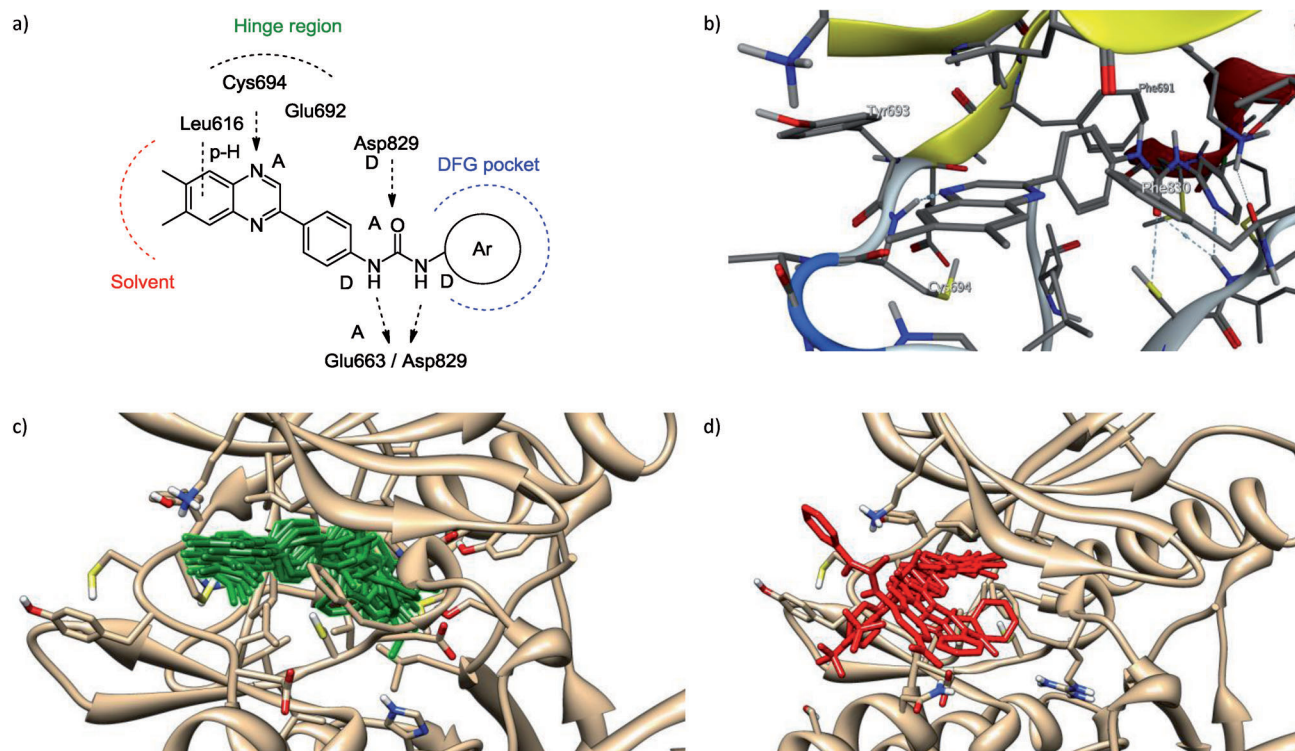


**Figure 5.** a),b) Docking study of compound **12b** using MOE 2013.08 and the known FLT3 crystal structure (PDB ID: 1RJ). c) Ensemble of compounds that fit into the hinge region and the DFG pocket (best-scoring pose). d) Compounds that could not be docked properly.<sup>[20]</sup>

the type II conformation was impossible (Figure 5). Various functional groups were omitted from the synthesis candidates, as they represent prodrug concepts and thus do not bind to the kinase in the present form (carboxylate) or are potentially toxic (phenols, thiophenol, anilines). Diamine derivatives were ranked with low priority, as they require regioselective synthesis (formation of regioisomers) and can be oxidized to toxic *para*-aminophenols that can modify cellular macromolecules as benzoquinone imines. Extended Lipinski parameters were used for the selection; therefore derivatives with  $\log P > 6.0$  and a  $M_r > 600$  Da were discarded. Finally, 18 derivatives were selected for synthesis (Table 2). As observed for **AG1295**, the quinoxaline motif was oriented toward the protein surface and the aromatic head groups were located in the DFG pocket for quinoxalines **12a–m**. Thus, similar interactions were identified within the ATP binding pocket of FLT3. The benzothiazole derivative **12i** and the phenoxy derivative **12m** are very lipophilic. However, larger hydrophobic and aromatic contact surfaces may lead to higher activity. The lowest lipophilicities are exhibited by the picolyl derivative **12d** and the pyridine derivative **12g**. They are likely to display better solvent solubility, as  $\pi$ -stacking interactions in the crystal are weakened by the benzylic position. Several potential interactions were identified between the quinoxaline scaffold and the hinge region. Strong hydrogen bonds were predicted between the nitrogen atom of the quinoxaline and C694, additionally to the hydrogen bond with E692. L616 forms a hydrogen– $\pi$  interaction with the quinoxaline. Furthermore, the donor–acceptor motif of the

urea group forms multiple interactions with residues D829, K644, and E661.

### Synthesis and in vitro pharmacology

The synthesis of compounds **12a–m** started with the preparation of arylglyoxal **7**, which was used for condensation to the quinoxaline scaffold. Glyoxal **7** was prepared by oxidation of its corresponding acetophenone **6** by using selenium dioxide (Scheme 1). The commercial 4,5-dimethylbenzene-1,2-diamine and glyoxal **7** reacted at 80 °C in *N,N*-dimethylformamide (DMF) within 1 h to form 2-arylquinoxaline derivative **8**, which was obtained in good yield (80%). Reduction of intermediate **8** into its corresponding amine **9** was carried out in the presence of iron and iron(III) chloride. The final compound **12a** was obtained by in situ coupling of amine **9** with isocyanate **10**.

Aniline **9** was treated with triphosgene under basic conditions to form isocyanate **13**, which was coupled in situ with the selected amines to obtain the final quinoxaline derivatives **12b–r** (Scheme 1). The reference compound **AG1295** was synthesized as described by Zall et al. via  $\alpha$ -ketoaldehydes starting from benzaldehyde and 4,5-dimethylbenzene-1,2-diamine.<sup>[21]</sup>

The obtained quinoxalines **12a–r** were tested for their ability to inhibit FLT3 kinase activity (Table 2). The assay results are in agreement with our previous docking studies. Thus, seven quinoxaline derivatives **12a–g** exhibited an FLT3 inhibitory activity of  $> 50\%$  at 100 nM. Interestingly, five of them, **12c–g**, contain a methylene bridge between the urea motifs and the aromatic

**Table 2.** FLT3 in vitro inhibitory activities of quinoxaline derivatives **12a–r** and their calculated chemical properties.

Compd	R	log <i>P</i> <sup>[a]</sup>	tPSA [Å] <sup>[a]</sup>	Inhib. [%] <sup>[b]</sup>
AG1295	–	4.28	24.7	37
12a		4.66	87.4	80
12b		4.69	78.2	76
12c		4.83	65.8	76
12d		3.49	78.2	72
12e		4.70	75.1	67
12f		4.60	84.3	65
12g		4.70	75.1	63
12h		3.42	78.2	42
12i		5.04	117.7	41
12j		5.71	78.2	20
12k		4.62	78.2	13
12l		4.76	65.9	12
12m		5.73	65.9	9
12n		5.24	65.9	9
12o		4.63	75.1	5
12p		6.35	75.1	3
12q		4.13	78.2	0

**Table 2.** (Continued)

Compd	R	log <i>P</i> <sup>[a]</sup>	tPSA [Å] <sup>[a]</sup>	Inhib. [%] <sup>[b]</sup>
12r		5.67	87.4	0

[a] The partition coefficient (log *P*) and topological polar surface area (tPSA) were calculated with ChemBioDraw Ultra (version 13.0.2). [b] Results are expressed as a percentage of the control specific activity (SA) determined against FLT3 at an inhibitor concentration of 100 nM; percent inhibition = [(100 – SA<sub>measured</sub>)/SA<sub>control</sub>] × 100.

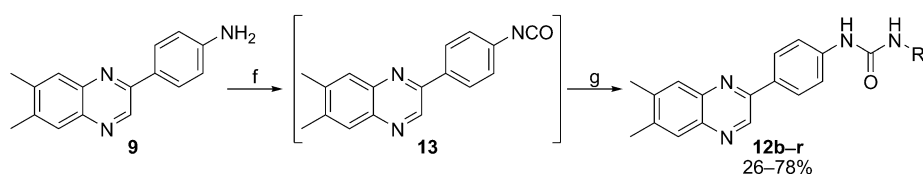
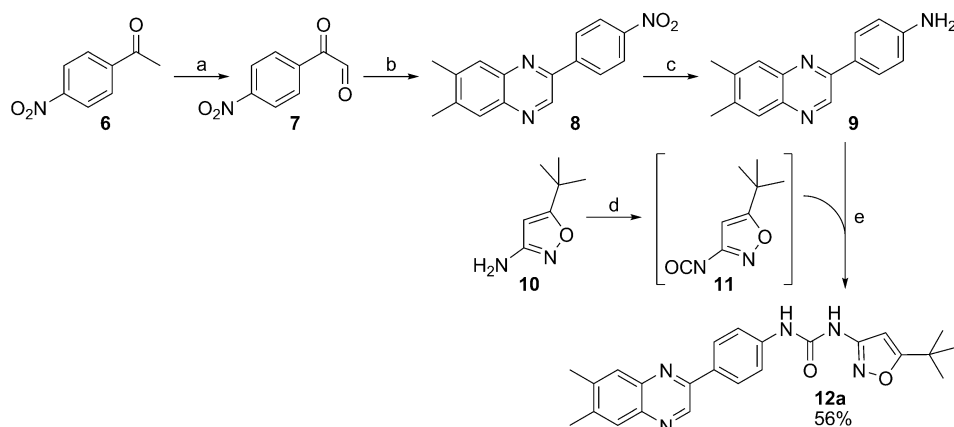
head groups. Comparison of compound **12c** and **12l** confirms the importance of the methylene bridge. Compound **12c** exhibited an FLT3 inhibition of 76% at 100 nM, whereas compound **12l**, which lacks this methylene group, exerts decreased inhibitory activity of merely 12%. One of the most potent compounds, **12a**, fuses structural elements from **AG1295** and quizartinib and exhibited an inhibition of 80% at 100 nM. The high activity of **12b** may be attributed to the chlorine substitution at the *para* position, which lowers the intramolecular hydrogen bonding capacity to the distal urea amine.

Compounds **12k** and **12q**, which lack this *para* substitution, exert no significant FLT3 inhibitory activity at 100 nM. Notably, differences in activity regarding closely related compounds cannot be explained by our modeling, for example, **12e** and **12p**. Next we investigated the role of the dimethyl quinoxaline moiety. Based on the most active and promising compound **12a**, we replaced the hydrophobic dimethyl groups by solubilizing methoxy or dimethoxy derivatives as present in **18a** and **18b** (Scheme 2). Thus, both nitro compounds **14a** and **14b** were reduced with Pd/C under hydrogen into their corresponding amines **15a** and **15b**, and were directly coupled with the previously synthesized glyoxal **7** to obtain the dimethoxy (**16a**) and methoxy (**16b**) intermediates, respectively. After reduction with Fe and FeCl<sub>3</sub> into their amino counterparts **17a** and **17b**, respectively, a solution of isocyanate **11** was added to give the desired products **18a** and **18b**.

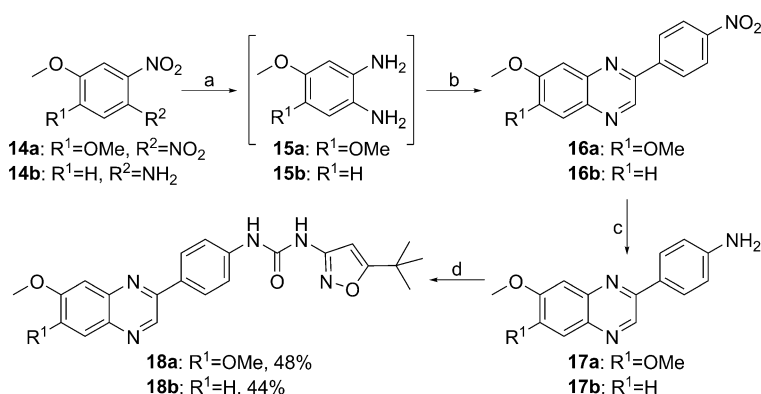
The results of the FLT3 in vitro assay indicated that both compounds exhibited lower inhibitory activity than that of derivative **12a** (Table 3). Nevertheless, the dimethoxy derivative **18a** exhibited better FLT3 in vitro inhibitory activity (51% inhibition at 100 nM) than compound **18b** with an inhibition of 30%.

The IC<sub>50</sub> values of compounds **12a–c** were determined for better differentiation. IC<sub>50</sub> values of 71 nM for **12a**, 32 nM for **12b**, and 88 nM for compound **12c** were observed, confirming the identification of a series of highly potent FLT3 inhibitors based on the quinoxaline scaffold (Table 4).

We further evaluated the most potent compound **12b** in a kinase selectivity panel at a concentration of 1 μM, including the FLT3 mutant D835Y (Figure 6). Remotely related kinases of other kinome families, such as LRRK2 (TKL family), GSK3-β (CMGC family), Pim1 kinase (CAMK family), ROCK1 (AGC



**Scheme 1.** Reactions and conditions: a)  $\text{SeO}_2$ , dioxane/ $\text{H}_2\text{O}$  3:1, 12 h,  $100^\circ\text{C}$ ; b) diamine, DMF, 1 h,  $80^\circ\text{C}$ ; c)  $\text{Fe}/\text{FeCl}_3$ , AcOH, EtOH, 1 h, reflux; d) triphosgene,  $\text{NEt}_3$ ,  $\text{CH}_2\text{Cl}_2$ , 1 h,  $-10^\circ\text{C}$ ; e) toluene, 2 h, reflux; f) triphosgene, sat.  $\text{NaHCO}_3$ ,  $\text{CH}_2\text{Cl}_2$ , 20 min, RT; g) amine, THF, 2 h, reflux.



**Scheme 2.** Reactions and conditions: a)  $\text{Pd}/\text{C}$ ,  $\text{H}_2$ ,  $\text{CH}_3\text{OH}$ , 4 h, RT; b) glyoxal **7**, DMF, 1 h,  $80^\circ\text{C}$ ; c)  $\text{Fe}/\text{FeCl}_3$ , AcOH,  $\text{CH}_3\text{OH}$ , 1 h, reflux; d) isocyanate **11**, toluene, 2 h, reflux.

**Table 3.** FLT3 in vitro inhibitory activity of compounds **18a** and **18b**.

Compd	$\text{R}^1$	$\log P^{[a]}$	Inhibition [%] <sup>[b]</sup>
<b>18a</b>	OMe	3.43	51
<b>18b</b>	H	3.56	30

[a] The partition coefficient ( $\log P$ ) was calculated with ChemBioDraw Ultra (version 13.0.2). [b] Results are expressed as a percentage of the control specific activity (SA) determined against FLT3 at an inhibitor concentration of 100 nM; percent inhibition =  $[(100 - \text{SA}_{\text{measured}}) / \text{SA}_{\text{control}}] \times 100$ .

embryos are transparent and develop outside the body.<sup>[23c,24]</sup> These features have established the zebrafish as a key model in toxicological and pharmacological research. Treatment of zebrafish with test drugs or chemicals may result in a change in

**Table 4.** FLT3 in vitro inhibitory activity of compounds **12a–c**.

Compd	$\text{IC}_{50}$ [nM]	Inhibition [%] <sup>[a]</sup>
<b>12a</b>	71	80
<b>12b</b>	32	76
<b>12c</b>	88	76

[a] Results are expressed as a percentage of the control specific activity determined against FLT3 at an inhibitor concentration of 100 nM; percent inhibition =  $[(100 - \text{SA}_{\text{measured}}) / \text{SA}_{\text{control}}] \times 100$ .

family), and MEK1 (STE family) are not inhibited, as are single members of the TK family (e.g., IGF1R, VEGFR2, Abl). Closely related kinases in the type III RTK family are inhibited, reaching from relatively weak inhibition of PDGFR $\alpha$  and PDGFR $\beta$  kinases to nearly equipotent inhibition of c-KIT kinase. PDGFR and especially KIT activity can be commonly observed for FLT3 inhibitors as quizartinib, based on high sequence identity (62%) and sequence similarity (77%). The FLT3 D835Y mutant destabilizes the inactive kinase conformation, a prerequisite for type II inhibitor binding. The mutant kinase is not inhibited by **12b**, which is indicative of type II ATP-competitive binding and is in accordance with in vitro data for other type II inhibitors.<sup>[12]</sup> Dual inhibition of FLT3 and c-KIT may offer clinical advantages.<sup>[22]</sup>

Next, we examined compound **12a** and **AG1295** for their in vivo activity on zebrafish embryo development. In the past decades the zebrafish (*Danio rerio*) has become a useful aquatic vertebrate model to study developmental mechanisms and to assess toxicological effects of chemicals and drugs; it is standardized internationally.<sup>[23]</sup> Indeed, the zebrafish has high fecundity (~60–200 eggs per spawning), rapid embryonic development (~3 days) and small size. The

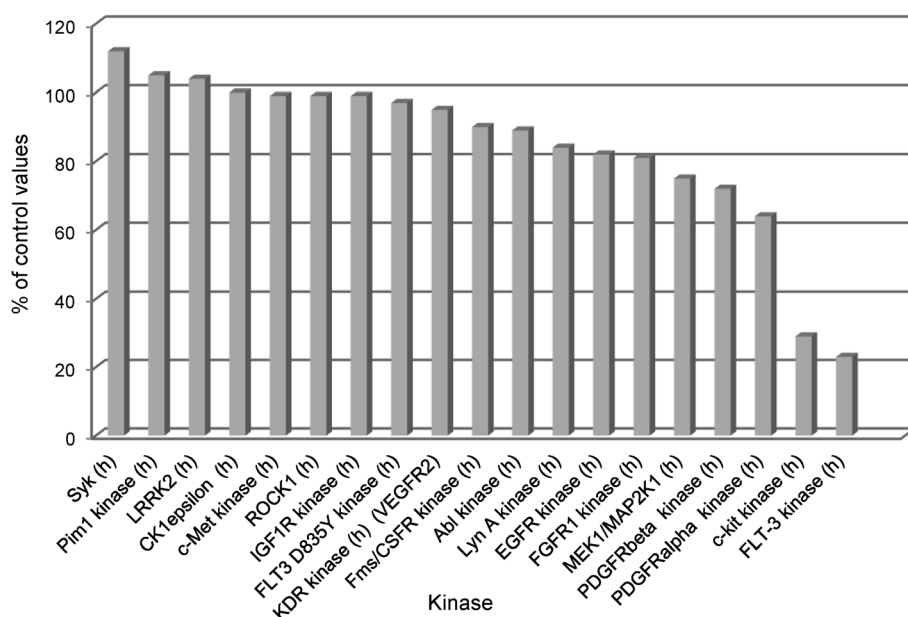


Figure 6. Kinase selectivity panel of compound **12b** at a concentration of 1  $\mu\text{M}$ .

phenotype. Therefore, conclusions can be drawn concerning the safety and permeability of the compounds in question.

In our zebrafish assay the embryos were collected and maintained in E3 medium at 28 °C. Compound **12a** was added at 24 hours post-fertilization (hpf), and the phenotypes were compared after 96 hpf (Figure 7). Lower concentrations of compound **12a** from 1 to 20  $\mu\text{M}$  did not reveal any abnormalities relative to control (Figure 7A–C). At concentrations of 30 and 40  $\mu\text{M}$ , the phenotypes changed, and 15% of the zebrafish displayed stunted and crooked tails (Figure 7D,E). After treating the zebrafish with compound **12a** at higher concentrations (50 and 100  $\mu\text{M}$ ), related but more pronounced phenotypes were observed. Stunted and crooked tails were observed in addition to the constrained circular movement. At 100  $\mu\text{M}$ , compound **12a** was observed to impart a developmental delay (50% of the zebrafish did not hatch), and all embryos exhibited abnormalities relative to the control (Figure 7H). In addition to phenotypic description, we monitored lethality in the zebrafish every 24 h up to 120 hpf by heartbeat observation (Figure 7). We observed that at lower concentrations (1–40  $\mu\text{M}$ ) the lethality in zebrafish embryos ranged from 0 to 10%. At 100  $\mu\text{M}$ , the survival rate decreased to 20%. Related phenotypes were observed for **AG1295**. At concentrations < 20  $\mu\text{M}$  the zebrafish embryos exhibited no abnormalities relative to control. Upon increasing concentration to 100  $\mu\text{M}$ , both stunted and crooked tails were more pronounced. **AG1295** also displayed similar lethality as observed for compound **12a**. Nevertheless, the zebrafish assay did not indicate any abnormalities for compound **12a** at concentrations < 20  $\mu\text{M}$ , and indicated no (1  $\mu\text{M}$ ) or weak cytotoxicity up to concentrations of 40  $\mu\text{M}$ . As quizartinib was reported to be nonlethal toward zebrafish embryos, the observed lethality may be due to off-target effects.<sup>[25]</sup>

## Conclusions

We sought an efficient in silico algorithm to optimize the fragment-sized FLT3 inhibitor **AG1295**. Substitution of the **AG1295** core with bisarylureas occupying the DFG pocket led to potent FLT3 inhibitors. Based on this hypothesis, we created an optimization algorithm to refine an in silico library by pharmacophore filtering using a diverse set of known inhibitors. Subsequent structure-based filtering led to optimized quinoxaline-based tyrosine kinase inhibitors. These in silico hits were synthesized and evaluated in biological assays resulting in tenfold increased inhibitory potency relative to that of **AG1295**. The most active compounds exhibit

$\text{IC}_{50}$  values of 71 nM (**12a**) and 32 nM (**12b**). Consequently, we evaluated the toxicity of compound **12a** against **AG1295** in our in vivo zebrafish embryo phenotype assay, observing no toxicity < 20  $\mu\text{M}$  for both compounds. Future studies will focus on the development of quinoxaline-based inhibitors of the active kinase state to overcome increasing resistance to type II inhibitors caused by the FLT3 D835Y mutation. Evaluation of future kinase inhibitors should focus on selectivity over even near family members and should aim for sustained inhibition in cellular assays and in vivo models for AML.

## Experimental Section

$^1\text{H}$  NMR spectra were recorded on a Bruker AC 300 spectrometer at 300 MHz and a Bruker AC 500 spectrometer at 500 MHz.  $^{13}\text{C}$  NMR spectra were recorded on a Bruker AC 300 spectrometer at 75 MHz and a Bruker AC 500 spectrometer at 125 MHz. Chemical shifts are reported in ppm and are calibrated to the particular solvent. Mass spectrometry was performed on a Bruker–Franzen Esquire LC mass spectrometer and a MAT 95 double focusing sector field MS instrument. Microwave experiments were carried out with a Biotage Initiator microwave apparatus. All microwave experiments were carried out in sealed microwave process vials using the standard absorbance level (300 W maximum power). Silica gel chromatography was carried out using Merck silica gel 60 (0.015–0.040 mm). High-performance liquid chromatography was carried out on an Agilent 1100 (column: reversed-phase, Zorbax Eclipse XDB-C<sub>8</sub>, 4.6 × 150 mm; 254 nm). The eluent was composed of: H<sub>2</sub>O (1% TFA) (A) and CH<sub>3</sub>CN (1% TFA) (B) with a gradient 30 → 90% B within 12 min. Automated flash chromatography was performed on a Teledyne ISCO Combi Flash RF 4X using H<sub>2</sub>O and CH<sub>3</sub>CN solvent mixtures. All commercially available reagents and solvents were purchased at ABCR, Acros, Sigma–Aldrich and VWR.

**2-(4-Nitrophenyl)-2-oxoacetaldehyde (7):** A suspension of SeO<sub>2</sub> (671 mg, 6.05 mmol) in dioxane (6 mL) and H<sub>2</sub>O (2 mL) was stirred at 55 °C until the solid dissolved, and then treated with 1-(4-nitro-

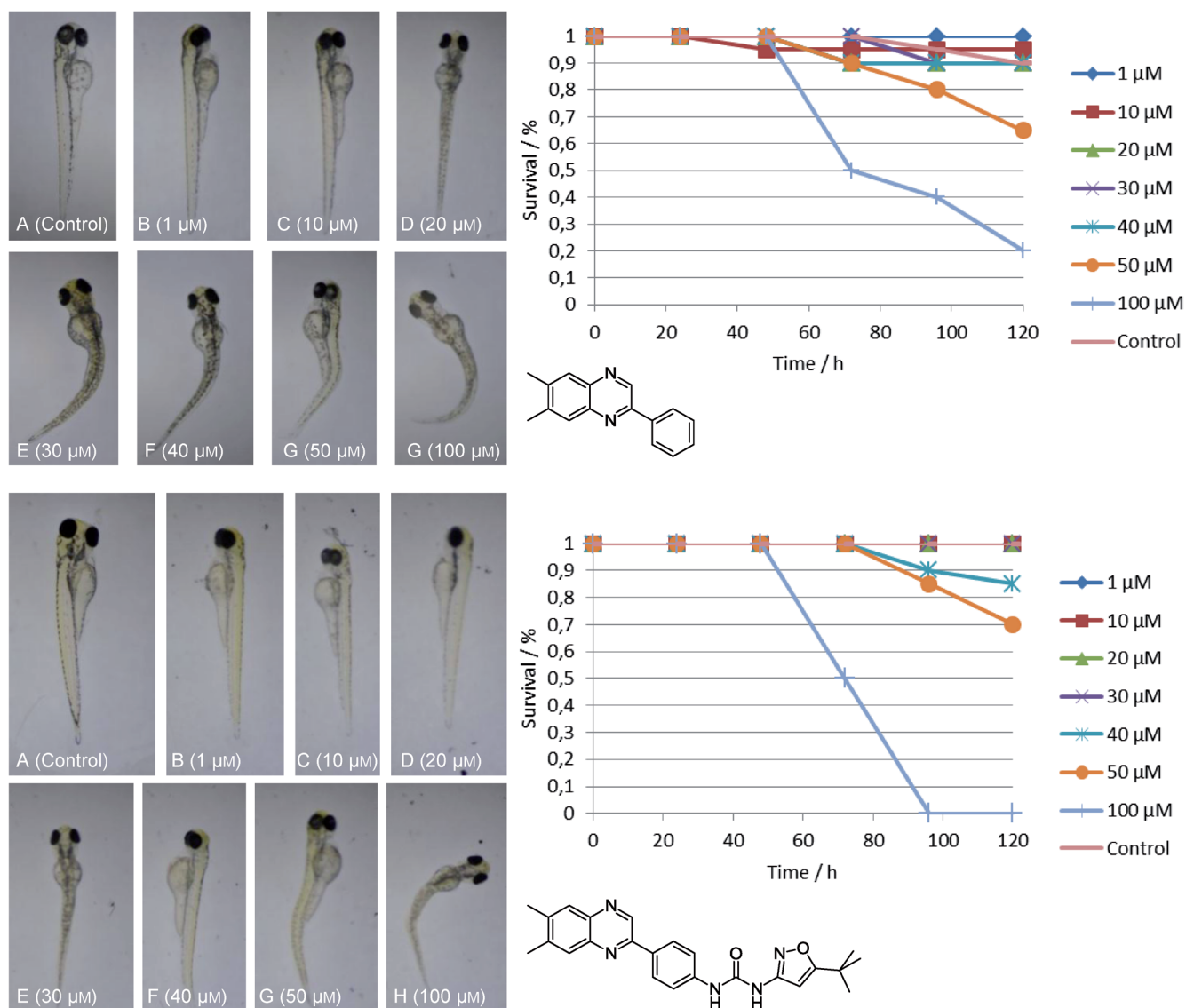


**Figure 7.** In vivo cytotoxicity toward zebrafish embryos and the survival rate at various time points for compound **12a** (top) and **AG1295** (bottom). Compound **12a** and **AG1295** were added 24 hours post-fertilization (hpf) to ten embryos in duplicates, and the phenotypes were compared after 96 hpf. A) Control embryo in 1% DMSO. B)–H) Zebrafish embryos treated with compound **12a** and **AG1295** at increasing concentrations of B) 1, C) 10, D) 20, E) 30, F) 40, G) 50, and H) 100  $\mu\text{M}$ .

phenyl)ethanone **6** (200 mg, 1.21 mmol). The mixture was stirred overnight at 100 °C. The black solid was filtered off and discarded, and the filtrate was concentrated in vacuo. The residue was diluted in EtOAc (20 mL), washed with H<sub>2</sub>O (15 mL) and saturated aq NaHCO<sub>3</sub> (15 mL), dried (MgSO<sub>4</sub>) and filtered, and the solvent was removed in vacuo. Purification by silica gel column chromatography (cyclohexane/EtOAc, 1:1) gave the title compound as a yellow solid (148 mg, 68%); HPLC:  $t_{\text{R}}=1.83$  min; <sup>1</sup>H NMR ([D<sub>6</sub>]DMSO, 300 MHz):  $\delta=8.41\text{--}8.21$  (m, 4H), 7.05 ppm (d, 2H,  $J=6.8$  Hz); <sup>13</sup>C NMR ([D<sub>6</sub>]DMSO, 75 MHz):  $\delta=195.3, 149.8, 138.5, 130.8, 123.5, 90.1$  ppm.

**6,7-Dimethyl-2-(4-nitrophenyl)quinoxaline (8):** A solution of 2-(4-nitrophenyl)-2-oxoacetaldehyde **7** (140 mg, 0.78 mmol) and 4,5-dimethylbenzene-1,2-diamine (106 mg, 0.78 mmol) in DMF (5 mL) was stirred for 2 h at 80 °C. After cooling to RT, H<sub>2</sub>O (3 mL) was added, and the obtained solid was isolated by filtration and dried to give the title compound as a light-yellow solid (174 mg, 80%);

HPLC:  $t_{\text{R}}=7.83$  min; <sup>1</sup>H NMR (CDCl<sub>3</sub>, 500 MHz):  $\delta=9.28$  (s, 1H), 8.41–8.36 (m, 4H), 7.96 (s, 2H), 2.55 ppm (s, 6H); <sup>13</sup>C NMR (CDCl<sub>3</sub>, 125 MHz):  $\delta=148.9, 148.7, 142.8, 142.4, 142.3, 141.7, 141.0, 140.2, 129.0, 128.3, 127.8, 124.4, 20.7, 20.6$  ppm.

**4-(6,7-Dimethylquinoxalin-2-yl)aniline (9):** Acetic acid (1.30 mL), Fe (190 mg, 3.39 mmol) and FeCl<sub>3</sub> (92 mg, 0.57 mmol) were added to a solution of 6,7-dimethyl-2-(4-nitrophenyl)quinoxaline **8** (158 mg, 0.57 mmol) in EtOH (7 mL), and the mixture was stirred for 1 h at 80 °C. After cooling to RT, the solvent was removed, and the residue was dissolved in EtOAc (30 mL) and washed with H<sub>2</sub>O (20 mL). The organic phase was dried (MgSO<sub>4</sub>) and filtered, and the solvent was removed in vacuo. Purification by silica gel column chromatography (CHCl<sub>3</sub>/CH<sub>3</sub>OH, 20:1) gave the title compound as a yellow solid (70 mg, 50%); HPLC:  $t_{\text{R}}=3.09$  min; <sup>1</sup>H NMR ([D<sub>6</sub>]DMSO, 500 MHz):  $\delta=9.28$  (s, 1H), 8.02 (d, 2H,  $J=8.6$  Hz), 7.77 (s, 2H), 6.71 (d, 2H,  $J=8.6$  Hz), 5.67 (s, 2H), 2.45 ppm (d, 6H,  $J=4.2$  Hz); <sup>13</sup>C NMR ([D<sub>6</sub>]DMSO, 125 MHz):  $\delta=151.0, 150.5, 142.0,$

141.9, 140.4, 140.2, 139.1, 139.3, 128.3, 127.7, 123.3, 113.8, 19.8, 19.6 ppm.

**1-(5-tert-Butylisoxazol-3-yl)-3-(4-(6,7-dimethylquinoxalin-2-yl)phenyl)urea (12a):** A solution of 5-tert-butylisoxazol-3-amine **10** (17 mg, 0.12 mmol) and triphosgene (10 mg, 0.12 mmol) in CH<sub>2</sub>Cl<sub>2</sub> (2 mL) was treated dropwise at -10 °C with a solution of Et<sub>3</sub>N (34 μL, 0.22 mmol) in CH<sub>2</sub>Cl<sub>2</sub> (0.5 mL). The mixture was stirred for 1 h at this temperature. Afterward, a solution of 4-(6,7-dimethylquinoxalin-2-yl)aniline **9** (30 mg, 0.12 mmol) in toluene (1 mL) was added, and the mixture was stirred for 2 h at 110 °C. After cooling to RT, H<sub>2</sub>O (5 mL) was added, and the aqueous mixture was extracted with EtOAc (3 × 10 mL). The combined organic layers were dried (MgSO<sub>4</sub>) and filtered, and the solvent was removed in vacuo. Purification by silica gel column chromatography (CHCl<sub>3</sub>/CH<sub>3</sub>OH, 25:1) gave the title compound as a light-yellow solid (28 mg, 56%); HPLC: *t*<sub>R</sub> = 8.00 min (95%); <sup>1</sup>H NMR ([D<sub>6</sub>]DMSO, 500 MHz): δ = 9.58 (s, 1H), 9.42 (s, 1H), 9.07 (s, 1H), 8.29–8.26 (m, 2H), 7.87 (d, 2H, *J* = 11.4 Hz), 7.68–7.65 (m, 2H), 6.54 (s, 1H), 2.49 (d, 6H, *J* = 3.0 Hz), 1.31 ppm (s, 9H); <sup>13</sup>C NMR ([D<sub>6</sub>]DMSO, 125 MHz): δ = 180.3, 158.2, 151.2, 149.6, 142.3, 140.9, 140.7, 140.3, 139.7, 139.7, 130.3, 127.9, 127.7, 118.5, 92.4, 28.3, 19.8, 19.7 ppm; MS (EI, 70 eV): *m/z* = 438 [M + Na]<sup>+</sup>; HRMS-EI: *m/z* [M]<sup>+</sup> calcd for C<sub>24</sub>H<sub>25</sub>N<sub>5</sub>O<sub>2</sub>: 415.2009, found: 415.20082.

**1-(4-Chloropyridin-2-yl)-3-(4-(6,7-dimethylquinoxalin-2-yl)phenyl)urea (12b):** A biphasic system of triphosgene (35 mg, 0.12 mmol) in CH<sub>2</sub>Cl<sub>2</sub> (3 mL) and saturated NaHCO<sub>3</sub> solution (15 mL) was treated dropwise with a solution of 4-(6,7-dimethylquinoxalin-2-yl)aniline **9** (84 mg, 0.34 mmol) in CH<sub>2</sub>Cl<sub>2</sub> (10 mL). The organic phase turned red, and the mixture was stirred until homogeneous. The reaction was stopped by separation of the organic phase, which was dried (MgSO<sub>4</sub>), filtered and concentrated in vacuo to give a red solid, which was used directly in the next step. The red solid was dissolved in THF (4 mL), and the mixture was added to a solution of 4-chloropyridin-2-amine (48 mg, 0.37 mmol) in THF (4 mL). The reaction was stirred at reflux for 2 h. After cooling to RT, the solvent was removed, and the residue was dissolved in a small amount of DMF, and H<sub>2</sub>O (1 mL) was added. The obtained precipitate was isolated by filtration and dried in vacuo to give the desired compound as a yellow solid (51 mg, 36%); HPLC: *t*<sub>R</sub> = 7.46 min (99%); <sup>1</sup>H NMR ([D<sub>6</sub>]DMSO, 500 MHz): δ = 10.21 (s, 1H), 9.64 (s, 1H), 9.45 (d, 1H, *J* = 1.2 Hz), 8.35–8.29 (m, 3H), 7.92–7.86 (m, 2H), 7.80 (d, 1H, *J* = 1.9 Hz), 7.77–7.71 (m, 2H), 7.19 (dd, 1H, *J* = 5.5, 1.9 Hz), 2.51–2.51 (m, 3H), 2.51–2.49 ppm (m, 3H); <sup>13</sup>C NMR ([D<sub>6</sub>]DMSO, 125 MHz): δ = 179.7, 153.7, 151.7, 149.6, 148.9, 144.1, 142.3, 140.7, 140.4, 139.8, 139.7, 130.4, 128.0, 127.7, 118.8, 118.4, 117.9, 111.3, 19.8, 19.8 ppm; MS (EI, 70 eV): *m/z* = 403 [M]<sup>+</sup>; HRMS-EI: *m/z* [M]<sup>+</sup> calcd for C<sub>22</sub>H<sub>18</sub>ClN<sub>5</sub>O: 403.1197, found: 403.12015.

**1-Benzyl-3-(4-(6,7-dimethylquinoxalin-2-yl)phenyl)urea (12c):** Starting from phenylmethanamine (26 μL, 0.24 mmol) and using the same procedure as described for **12b**, the title compound was obtained as a yellow solid (35 mg, 42%); HPLC: *t*<sub>R</sub> = 7.24 min (96%); <sup>1</sup>H NMR ([D<sub>6</sub>]DMSO, 500 MHz): δ = 9.39 (s, 1H), 8.88 (s, 1H), 8.22–8.19 (m, 2H), 7.84 (d, 2H, *J* = 9.1 Hz), 7.64–7.61 (m, 2H), 7.37–7.32 (m, 4H), 7.27–7.24 (m, 1H), 6.74 (t, 1H, *J* = 5.9 Hz), 4.33 (d, 2H, *J* = 5.9 Hz), 2.47 ppm (d, 6H, *J* = 3.0 Hz); <sup>13</sup>C NMR ([D<sub>6</sub>]DMSO, 125 MHz): δ = 154.9, 149.8, 142.5, 142.2, 140.6, 140.5, 140.1, 139.6, 139.4, 128.8, 128.3, 127.9, 127.8, 127.7, 127.1, 126.7, 117.7, 42.8, 19.8, 19.7 ppm; MS (EI, 70 eV): *m/z* = 382 [M]<sup>+</sup>.

**1-(4-(6,7-Dimethylquinoxalin-2-yl)phenyl)-3-(pyridin-3-ylmethyl)urea (12d):** Starting from pyridin-3-ylmethanamine (33 mg,

0.30 mmol) and using the same procedure as described for **12b**, the title compound **12d** was obtained as a colorless solid (84 mg, 78%); HPLC: *t*<sub>R</sub> = 3.76 min (100%); <sup>1</sup>H NMR ([D<sub>6</sub>]DMSO, 500 MHz): δ = 9.39 (s, 1H), 9.00 (s, 1H), 8.58 (d, 1H, *J* = 2.2 Hz), 8.49 (dd, 1H, *J* = 4.8, 1.6 Hz), 8.26–8.19 (m, 2H), 7.84 (d, 2H, *J* = 8.5 Hz), 7.76 (dt, 1H, *J* = 7.8, 2.0 Hz), 7.68–7.59 (m, 2H), 7.39 (dd, 1H, *J* = 7.8, 4.8 Hz), 6.89 (t, 1H, *J* = 6.0 Hz), 4.39 (d, 2H, *J* = 5.9 Hz), 2.49 ppm (s, 6H); <sup>13</sup>C NMR ([D<sub>6</sub>]DMSO, 125 MHz): δ = 155.0, 149.8, 148.7, 148.0, 142.4, 142.2, 140.6, 140.4, 139.6, 139.4, 135.7, 134.99, 129.0, 127.9, 127.8, 127.7, 123.4, 117.8, 40.5, 19.8, 19.7 ppm; MS (EI, 70 eV): *m/z* = 383 [M]<sup>+</sup>.

**1-(4-(6,7-Dimethylquinoxalin-2-yl)phenyl)-3-(4-methoxybenzyl)urea (12e):** Starting from (4-methoxyphenyl)methanamine (31 μL, 0.24 mmol) and using the same procedure as described for **12b**, the title compound **12e** was obtained as a yellow solid (31 mg, 34%); HPLC: *t*<sub>R</sub> = 7.21 min (97%); <sup>1</sup>H NMR ([D<sub>6</sub>]DMSO, 500 MHz): δ = 9.39 (s, 1H), 8.83 (s, 1H), 8.21–8.19 (m, 2H), 7.84 (d, 2H, *J* = 9.1 Hz), 7.63–7.60 (m, 2H), 7.27–7.24 (m, 2H), 6.92–6.89 (m, 2H), 6.56 (t, 1H, *J* = 5.8 Hz), 4.25 (d, 2H, *J* = 5.8 Hz), 3.74 (s, 3H), 2.48 ppm (d, 6H, *J* = 3.0 Hz); <sup>13</sup>C NMR ([D<sub>6</sub>]DMSO, 125 MHz): δ = 158.2, 154.9, 149.9, 142.5, 142.2, 140.6, 140.4, 139.6, 139.4, 132.0, 128.8, 128.5, 127.9, 127.8, 127.7, 117.7, 113.7, 55.1, 42.3, 19.8, 19.7 ppm; MS (EI, 70 eV): *m/z* = 412 [M]<sup>+</sup>.

**1-(Benzo[d][1,3]dioxol-5-ylmethyl)-3-(4-(6,7-dimethylquinoxalin-2-yl)phenyl)urea (12f):** The title compound **12f** was obtained as a yellow solid (35 mg, 37%) using the same procedure as described for **12b** starting from benzo[d][1,3]dioxol-5-ylmethanamine (36 mg, 0.24 mmol); HPLC: *t*<sub>R</sub> = 7.21 min (96%); <sup>1</sup>H NMR ([D<sub>6</sub>]DMSO, 500 MHz): δ = 9.39 (s, 1H), 8.84 (s, 1H), 8.22–8.19 (m, 2H), 7.84 (d, 2H, *J* = 9.2 Hz), 7.63–7.60 (m, 2H), 6.89 (d, 1H, *J* = 1.6 Hz), 6.87 (d, 1H, *J* = 7.9 Hz), 6.80 (dd, 1H, *J* = 7.9, 1.6 Hz), 6.67 (t, 1H, *J* = 5.9 Hz), 5.98 (s, 2H), 4.23 (d, 2H, *J* = 5.9 Hz), 2.47 ppm (d, 6H, *J* = 3.0 Hz); <sup>13</sup>C NMR ([D<sub>6</sub>]DMSO, 125 MHz): δ = 154.9, 149.9, 147.2, 146.0, 142.5, 142.2, 140.6, 140.4, 139.6, 139.4, 134.1, 128.8, 127.9, 127.8, 127.7, 120.4, 117.7, 108.0, 107.9, 100.9, 42.6, 19.8, 19.7 ppm; MS (EI, 70 eV): *m/z* = 426 [M]<sup>+</sup>.

**1-(4-(6,7-Dimethylquinoxalin-2-yl)phenyl)-3-(3-methoxybenzyl)urea (12g):** The title compound **12g** was obtained as a yellow solid (25 mg, 26%) using the same procedure as described for **12b** starting from 3-methoxybenzylamine (32 mg, 0.233 mmol); HPLC: *t*<sub>R</sub> = 7.27 min (95%); <sup>1</sup>H NMR ([D<sub>6</sub>]DMSO, 500 MHz): δ = 9.45 (s, 1H), 8.95 (s, 1H), 8.27 (d, *J* = 8.8 Hz, 2H), 7.92 (s, 1H), 7.90 (s, 1H), 7.68 (d, *J* = 8.8 Hz, 2H), 7.32 (t, *J* = 7.8 Hz, 1H), 7.00–6.92 (m, 1H), 6.91–6.86 (m, 1H), 6.79 (t, *J* = 6.0 Hz, 1H), 4.37 (d, *J* = 5.9 Hz, 2H), 3.81 (s, 3H), 2.54 (s, 3H), 2.54 ppm (s, 3H); <sup>13</sup>C NMR ([D<sub>6</sub>]DMSO, 125 MHz): δ = 159.33, 154.96, 149.87, 142.48, 142.22, 140.37, 139.61, 139.46, 129.40, 128.87, 127.87, 127.80, 127.70, 119.28, 117.74, 116.47, 112.84, 112.09, 54.99, 42.73, 39.82, 19.82, 19.72, 19.57 ppm; MS (EI, 70 eV): *m/z* = 412 [M]<sup>+</sup>.

**1-(4-(6,7-Dimethylquinoxalin-2-yl)phenyl)-3-(pyridin-3-yl)urea (12h):** The title compound **12h** was obtained as a yellow solid (84 mg, 67%) using the same procedure as described for **12b** starting from pyridin-3-amine (32 mg, 0.34 mmol); HPLC: *t*<sub>R</sub> = 4.36 min (94%); <sup>1</sup>H NMR ([D<sub>6</sub>]DMSO, 500 MHz): δ = 9.42 (s, 1H), 9.11 (s, 1H), 8.93 (s, 1H), 8.64 (d, 1H, *J* = 2.3 Hz), 8.28–8.25 (m, 2H), 8.21 (dd, 1H, *J* = 4.6, 1.1 Hz), 7.98–7.96 (m, 1H), 7.86 (d, 2H, *J* = 10.6 Hz), 7.70–7.67 (m, 2H), 7.33 (dd, 1H, *J* = 8.3, 4.7 Hz), 2.48 ppm (d, 6H, *J* = 3.4 Hz); <sup>13</sup>C NMR ([D<sub>6</sub>]DMSO, 125 MHz): δ = 152.4, 149.7, 143.1, 142.2, 141.4, 140.7, 140.3, 140.2, 139.7, 139.6, 136.2, 129.8, 127.9, 127.7, 125.3, 123.6, 118.4, 19.8, 19.7 ppm; MS (ES, 70 eV): *m/z* = 369 [M]<sup>+</sup>.

**1-(4-(6,7-Dimethylquinoxalin-2-yl)phenyl)-3-(4-methyl-3-nitrophenyl)urea (12i):** The title compound **12i** was obtained as a light-brown solid (65 mg, 45%) using the same procedure as described for **12b** starting from 4-methyl-3-nitroaniline (52 mg, 0.34 mmol); HPLC:  $t_R = 8.03$  min (95%);  $^1\text{H NMR}$  ( $[\text{D}_6]\text{DMSO}$ , 500 MHz):  $\delta = 9.42$  (s, 1H), 9.14 (s, 1H), 9.09 (s, 1H), 8.30 (d, 1H,  $J = 2.3$  Hz), 8.28–8.25 (m, 2H), 7.86 (d, 2H,  $J = 11.9$  Hz), 7.70–7.76 (m, 2H), 7.59 (dd, 1H,  $J = 8.3, 2.3$  Hz), 7.42 (d, 1H,  $J = 8.5$  Hz), 2.48 (d, 6H,  $J = 3.3$  Hz), 2.46 ppm (s, 3H);  $^{13}\text{C NMR}$  ( $[\text{D}_6]\text{DMSO}$ , 125 MHz):  $\delta = 152.2, 149.7, 148.8, 142.3, 141.3, 140.7, 140.3, 139.7, 139.6, 138.5, 133.0, 129.9, 127.9, 127.9, 127.7, 125.7, 123.1, 118.5, 113.4, 19.8, 19.7, 18.9$  ppm; MS (ES, 70 eV):  $m/z = 469$   $[M]^+$ .

**1-(Benzo[d]thiazol-2-yl)-3-(4-(6,7-dimethylquinoxalin-2-yl)phenyl)urea (12j):** The title compound **12j** was obtained as a red solid (51 mg, 43%) using the same procedure as described for **12b** starting from benzo[d]thiazol-2-amine (45 mg, 0.30 mmol); HPLC:  $t_R = 7.89$  min (96%);  $^1\text{H NMR}$  ( $[\text{D}_6]\text{DMSO}$ , 500 MHz):  $\delta = 9.84$  (s, 1H), 9.45 (s, 1H), 8.37–8.30 (m, 2H), 8.30 (s, 1H), 7.93 (dd, 1H,  $J = 7.9, 1.1$  Hz), 7.89 (d, 1H,  $J = 16.1$  Hz), 7.82–7.74 (m, 2H), 7.68 (d, 1H,  $J = 8.0$  Hz), 7.45–7.40 (m, 1H), 7.30–7.25 (m, 1H), 2.50 (s, 3H), 2.49 ppm (s, 3H);  $^{13}\text{C NMR}$  ( $[\text{D}_6]\text{DMSO}$ , 125 MHz):  $\delta = 159.8, 152.5, 149.6, 147.4, 142.3, 140.8, 140.6, 140.35, 139.7, 130.9, 130.6, 128.0, 127.7, 126.0, 122.9, 121.6, 119.1, 118.7, 19.8, 19.8$  ppm; MS (EI, 70 eV):  $m/z = 425$   $[M]^+$ .

**1-(4-(6,7-Dimethylquinoxalin-2-yl)phenyl)-3-(5-methylpyridin-2-yl)urea (12k):** The title compound **12k** was obtained as a yellow solid (52 mg, 51%) using the same procedure as described for **12b** starting from 5-methylpyridin-2-amine (31 mg, 0.29 mmol); HPLC:  $t_R = 5.44$  min (96%);  $^1\text{H NMR}$  ( $[\text{D}_6]\text{DMSO}$ , 500 MHz):  $\delta = 10.61$  (s, 1H), 9.35 (d, 2H,  $J = 5.0$  Hz), 8.26–8.17 (m, 2H), 8.10–8.02 (m, 1H), 7.79 (d, 2H,  $J = 13.5$  Hz), 7.71–7.62 (m, 2H), 7.54 (dd, 1H,  $J = 8.5, 2.3$  Hz), 7.39 (d, 1H,  $J = 8.4$  Hz), 2.42 (s, 3H), 2.41 (s, 3H), 2.18 ppm (s, 3H);  $^{13}\text{C NMR}$  ( $[\text{D}_6]\text{DMSO}$ , 125 MHz):  $\delta = 152.1, 150.6, 149.7, 146.5, 142.3, 141.1, 140.7, 140.4, 139.7, 139.6, 139.2, 136.1, 130.1, 127.9, 127.7, 126.5, 118.8, 111.6, 19.8, 19.7, 17.1$  ppm; MS (EI, 70 eV):  $m/z = 384$   $[M]^+$ .

**1-(4-(6,7-Dimethylquinoxalin-2-yl)phenyl)-3-phenylurea (12l):** The title compound **12l** was obtained as a red solid (35 mg, 32%) using the same procedure as described for **12b** starting from aniline (30 mg, 0.32 mmol); HPLC:  $t_R = 7.31$  min (95%);  $^1\text{H NMR}$  ( $[\text{D}_6]\text{DMSO}$ , 500 MHz):  $\delta = 9.43$  (s, 1H), 9.09 (s, 1H), 8.87 (s, 1H), 8.27 (d, 2H,  $J = 8.8$  Hz), 7.88 (dd, 2H,  $J = 11.9, 1.1$  Hz), 7.69 (d, 2H,  $J = 8.8$  Hz), 7.54–7.47 (m, 2H), 7.32 (dd, 2H,  $J = 8.5, 7.3$  Hz), 7.01 (tt, 1H,  $J = 7.4, 1.2$  Hz), 2.50 ppm (s, 6H);  $^{13}\text{C NMR}$  ( $[\text{D}_6]\text{DMSO}$ , 125 MHz):  $\delta = 152.4, 149.8, 142.2, 141.8, 140.7, 140.4, 139.7, 139.6, 139.5, 129.5, 128.8, 127.8, 127.7, 122.0, 118.3, 118.2, 19.8, 19.7$  ppm; MS (EI, 70 eV):  $m/z = 386$   $[M]^+$ .

**1-(2,6-Dimethylphenyl)-3-(4-(6,7-dimethylquinoxalin-2-yl)phenyl)urea (12m):** The title compound **12m** was obtained as a brown solid (81 mg, 42%) using the same procedure as described for **12b** starting from 2,6-dimethylaniline (59 mg, 0.49 mmol); HPLC:  $t_R = 7.41$  min (99%);  $^1\text{H NMR}$  ( $[\text{D}_6]\text{DMSO}$ , 500 MHz):  $\delta = 9.42$  (s, 1H), 9.24 (s, 1H), 8.25 (dd,  $J = 9.0, 2.8$  Hz, 2H), 7.98 (s, 1H), 7.87 (d,  $J = 10.5$  Hz, 2H), 7.72–7.66 (m, 2H), 6.98 (d,  $J = 7.4$  Hz, 1H), 6.80 (t,  $J = 7.5$  Hz, 1H), 2.50 (s, 3H), 2.49 (s, 3H), 2.25 ppm (s, 3H);  $^{13}\text{C NMR}$  ( $[\text{D}_6]\text{DMSO}$ , 125 MHz):  $\delta = 152.96, 149.85, 142.40, 142.24, 140.67, 140.37, 139.63, 139.48, 135.53, 135.12, 129.05, 128.36, 127.88, 127.81, 127.71, 126.02, 117.88, 19.82, 18.25, 17.69$  ppm; MS (EI, 70 eV):  $m/z = 396$   $[M]^+$ .

**1-(4-(6,7-Dimethylquinoxalin-2-yl)phenyl)-3-o-tolylurea (12n):** The title compound **12n** was obtained as a brown solid (81 mg,

48%) using the same procedure as described for **12b** starting from *o*-toluidine (47 mg, 0.44 mmol); HPLC:  $t_R = 7.24$  min (98%);  $^1\text{H NMR}$  ( $[\text{D}_6]\text{DMSO}$ , 500 MHz):  $\delta = 9.54$  (s, 1H), 9.34 (s, 1H), 8.21–8.17 (m, 2H), 8.14 (s, 1H), 7.78 (m, 2H), 7.65–7.59 (m, 2H), 7.12 (m, 1H), 7.08 (m, 1H), 6.96 (t,  $J = 7.2$  Hz, 1H), 6.90 (t,  $J = 7.3$  Hz, 1H), 2.42 (s, 3H), 2.41 (s, 3H), 2.22 ppm (s, 3H);  $^{13}\text{C NMR}$  ( $[\text{D}_6]\text{DMSO}$ , 125 MHz):  $\delta = 152.57, 149.80, 142.24, 142.00, 140.68, 140.37, 139.65, 139.53, 137.20, 130.83, 130.19, 129.34, 127.90, 127.70, 126.84, 126.11, 122.87, 121.24, 117.97, 17.98, 17.03, 8.52$  ppm; MS (EI, 70 eV):  $m/z = 382$   $[M]^+$ .

**1-(4-(6,7-Dimethylquinoxalin-2-yl)phenyl)-3-(2-methoxyphenyl)urea (12o):** The title compound **12o** was obtained as a brown solid (88 mg, 57%) using the same procedure as described for **12b** starting from 2-anisidine (47.9 mg, 0.389 mmol); HPLC:  $t_R = 7.84$  min (95%);  $^1\text{H NMR}$  ( $[\text{D}_6]\text{DMSO}$ , 500 MHz):  $\delta = 9.66$  (s, 1H), 9.46 (s, 1H), 8.38 (s, 1H), 8.31 (d,  $J = 8.8$  Hz, 1H), 8.21 (dd,  $J = 7.9, 1.7$  Hz, 1H), 7.94–7.89 (m, 1H), 7.73 (d,  $J = 8.7$  Hz, 1H), 7.10 (dd,  $J = 8.1, 1.5$  Hz, 1H), 7.03 (td,  $J = 7.8, 1.7$  Hz, 1H), 6.98 (td,  $J = 7.7, 1.5$  Hz, 1H), 3.96 (s, 3H), 2.54 (s, 3H), 2.53 ppm (s, 3H);  $^{13}\text{C NMR}$  ( $[\text{D}_6]\text{DMSO}$ , 125 MHz):  $\delta = 152.19, 149.78, 147.75, 142.24, 141.81, 140.70, 140.37, 139.67, 139.57, 129.49, 128.41, 127.94, 127.89, 127.70, 122.07, 120.56, 118.43, 117.96, 110.80, 55.81, 39.99, 19.82, 19.73$  ppm; MS (EI, 70 eV):  $m/z = 398$   $[M]^+$ .

**1-(4-(6,7-Dimethylquinoxalin-2-yl)phenyl)-3-(4-(trifluoromethoxy)benzyl)urea (12p):** The title compound **12p** was obtained as an orange solid (109 mg, 54%) using the same procedure as described for **12b** starting from 4-trifluoromethoxybenzylamine (78 mg, 0.41 mmol); HPLC:  $t_R = 7.97$  min (95%);  $^1\text{H NMR}$  ( $[\text{D}_6]\text{DMSO}$ , 500 MHz):  $\delta = 9.40$  (s, 1H), 8.96 (s, 1H), 8.22 (d,  $J = 8.8$  Hz, 2H), 7.86 (d,  $J = 9.0$  Hz, 2H), 7.64 (d,  $J = 8.8$  Hz, 2H), 7.47 (d,  $J = 8.7$  Hz, 2H), 7.36 (d,  $J = 8.0$  Hz, 2H), 6.84 (t,  $J = 5.9$  Hz, 1H), 4.38 (d,  $J = 5.9$  Hz, 2H), 2.49 (s, 3H), 2.49 ppm (s, 3H);  $^{13}\text{C NMR}$  ( $[\text{D}_6]\text{DMSO}$ , 125 MHz):  $\delta = 154.99, 149.85, 147.13, 142.41, 142.21, 141.47, 140.65, 140.36, 139.85, 139.61, 139.46, 128.92, 127.87, 127.78, 127.69, 120.92, 117.79, 42.09, 19.81, 19.71$  ppm; MS (EI, 70 eV):  $m/z = 466$   $[M]^+$ .

**1-(4-(6,7-Dimethylquinoxalin-2-yl)phenyl)-3-(pyridin-2-yl)urea (12q):** The title compound **12q** was obtained as a green solid (45 mg, 36%) using the same procedure as described for **12b** starting from pyridin-2-amine (32 mg, 0.34 mmol); HPLC:  $t_R = 5.12$  min (92%);  $^1\text{H NMR}$  ( $[\text{D}_6]\text{DMSO}$ , 500 MHz):  $\delta = 10.73$  (s, 1H), 9.52 (s, 1H), 9.43 (s, 1H), 8.33–8.27 (m, 3H), 7.87 (d, 2H,  $J = 14.6$  Hz), 7.79–7.73 (m, 3H), 7.54 (d, 1H,  $J = 8.4$  Hz), 7.05–7.03 (m, 1H), 7.49 ppm (d, 6H,  $J = 3.4$  Hz);  $^{13}\text{C NMR}$  ( $[\text{D}_6]\text{DMSO}$ , 125 MHz):  $\delta = 152.7, 152.0, 149.7, 146.9, 142.3, 141.0, 140.7, 140.3, 139.7, 139.6, 138.6, 130.2, 127.9, 127.7, 118.8, 117.7, 112.0, 19.8, 19.7$  ppm; MS (EI, 70 eV):  $m/z = 369$   $[M]^+$ .

**1-(4-(6,7-Dimethylquinoxalin-2-yl)phenyl)-3-(3-phenoxy-pyridin-2-yl)urea (12r):** The title compound **12r** was obtained as a yellow solid (63 mg, 42%) using the same procedure as described for **12b** starting from 3-phenoxy-pyridin-2-amine (64 mg, 0.35 mmol); HPLC:  $t_R = 7.27$  min (95%);  $^1\text{H NMR}$  ( $[\text{D}_6]\text{DMSO}$ , 500 MHz):  $\delta = 11.95$  (s, 1H), 9.46 (s, 1H), 8.37–8.25 (m, 3H), 8.00 (dd, 1H,  $J = 5.0, 1.4$  Hz), 7.95–7.87 (m, 2H), 7.84 (d, 1H,  $J = 8.8$  Hz), 7.59 (d, 1H,  $J = 1.5$  Hz), 7.55 (dd, 1H,  $J = 8.1, 1.4$  Hz), 7.48–7.41 (m, 2H), 7.40–7.35 (m, 1H), 7.09 (dd, 1H,  $J = 8.0, 5.0$  Hz), 5.31 (s, 2H), 2.52 (s, 3H), 2.51 ppm (s, 3H);  $^{13}\text{C NMR}$  ( $[\text{D}_6]\text{DMSO}$ , 125 MHz):  $\delta = 175.1, 171.8, 167.4, 166.1, 161.0, 150.7, 143.1, 142.4, 140.8, 140.0, 137.1, 136.1, 128.5, 128.2, 128.00, 127.8, 123.2, 121.2, 119.9, 119.4, 117.9, 112.9, 109.2, 19.8, 19.8$  ppm.

**6,7-Dimethoxy-2-(4-nitrophenyl)quinoxaline (16a):** Pd/C (10%, 30 mg) was added under argon to a stirred solution of 1,2-dime-

thoxy-4,5-dinitrobenzene **14a** (100 mg, 0.44 mmol) in CH<sub>3</sub>OH (5 mL). The mixture was flushed with hydrogen and stirred 4 h at RT. Afterward the suspension was filtered through a pad of Celite and the solvent was concentrated in vacuo to 1 mL. This solution was added to a second solution of 2-(4-nitrophenyl)-2-oxoacetaldehyde **7** (74 mg, 0.45 mmol) in DMF (1.5 mL) and stirred for 1 h at 80 °C. After cooling to RT, H<sub>2</sub>O (1 mL) was added, and the obtained brown solid was filtered, dried and gave 61 mg (44%); HPLC:  $t_R$  = 6.87 min; <sup>1</sup>H NMR (CDCl<sub>3</sub>, 500 MHz):  $\delta$  = 9.18 (s, 1H), 8.40 (m, 2H), 8.45 (m, 2H), 7.44 (d, 2H,  $J$  = 3.0 Hz), 4.11 ppm (d, 6H,  $J$  = 2.5 Hz); <sup>13</sup>C NMR (CDCl<sub>3</sub>, 125 MHz):  $\delta$  = 154.0, 154.0, 148.7, 147.2, 143.2, 140.0, 139.8, 139.4, 128.0, 124.4, 107.1, 106.4, 56.7, 56.7 ppm.

**4-(6,7-Dimethoxyquinoxalin-2-yl)aniline (17a)**: Acetic acid (0.45 mL), Fe (57 mg, 1.02 mmol) and FeCl<sub>3</sub> (57 mg, 0.17 mmol) were added to a solution of 6,7-dimethoxy-2-(4-nitrophenyl)quinoxaline **16a** (53 mg, 0.17 mmol) in EtOH (2.5 mL) and stirred for 1 h at 80 °C. After cooling to RT, the obtained brown solid was filtered and dried. The filtrate was extracted with CH<sub>2</sub>Cl<sub>2</sub> (3 × 10 mL). The combined organic layers were dried (MgSO<sub>4</sub>), filtered and the solvent was removed in vacuo to give 46 mg (96%) of brown solid and was used without further purification; HPLC:  $t_R$  = 1.73 min; <sup>1</sup>H NMR ([D<sub>6</sub>]DMSO, 500 MHz):  $\delta$  = 9.17 (s, 1H), 8.00 (d, 2H,  $J$  = 8.4 Hz), 7.35 (d, 2H,  $J$  = 4.8 Hz), 6.70 (d, 2H,  $J$  = 8.4 Hz), 5.59 (s, 2H), 3.96 ppm (d, 6H,  $J$  = 8.9 Hz).

**1-(5-tert-Butylisoxazol-3-yl)-3-(4-(6,7-dimethoxyquinoxalin-2-yl)phenyl)urea (18a)**: To solution of 5-tert-butylisoxazol-3-amine **10** (30 mg, 0.21 mmol) in CH<sub>2</sub>Cl<sub>2</sub> (2 mL) and triphosgene (16 mg, 0.05 mmol) was added dropwise at -10 °C a solution of Et<sub>3</sub>N (58  $\mu$ L, 0.42 mmol) in CH<sub>2</sub>Cl<sub>2</sub> (1 mL). The mixture was stirred for 1 h at this temperature. Afterward a solution of 4-(6,7-dimethoxyquinoxalin-2-yl)aniline **17a** (46 mg, 0.16 mmol) in toluene (1.5 mL) was added and the mixture was stirred for 2 h at 110 °C. After cooling to RT, H<sub>2</sub>O (10 mL) was added and extracted with EtOAc (3 × 10 mL). The combined organic layers were dried (MgSO<sub>4</sub>), filtered and the solvent was removed in vacuo. After purification by flash chromatography (RediSep Column: 13 g C<sub>18</sub> gold, H<sub>2</sub>O/CH<sub>3</sub>CN: 0% → 95% CH<sub>3</sub>CN in 12 min) 23 mg (48%) of a yellow solid was obtained; HPLC:  $t_R$  = 7.17 min (100%); <sup>1</sup>H NMR ([D<sub>6</sub>]DMSO, 500 MHz):  $\delta$  = 9.58 (s, 1H), 9.30 (s, 1H), 9.04 (s, 1H), 8.26–8.23 (m, 2H), 7.67–7.64 (m, 2H), 7.42 (d, 2H,  $J$  = 7.4 Hz), 6.54 (s, 1H), 3.99 (d, 6H,  $J$  = 7.2 Hz), 1.31 ppm (s, 9H); <sup>13</sup>C NMR ([D<sub>6</sub>]DMSO, 125 MHz):  $\delta$  = 180.3, 158.3, 152.8, 152.1, 151.2, 148.1, 140.5, 140.1, 138.6, 137.9, 130.5, 127.5, 118.5, 106.7, 106.6, 92.5, 56.0, 28.3 ppm; MS (EI, 70 eV):  $m/z$  = 447 [M]<sup>+</sup>.

**7-Methoxy-2-(4-nitrophenyl)quinoxaline (16b)**: Pd/C (10%, 54 mg) was added under argon to a stirred solution of 4-methoxy-2-nitroaniline **14b** (180 mg, 1.07 mmol) in CH<sub>3</sub>OH (8 mL). The mixture was flushed with hydrogen and stirred 4 h at RT. Afterward the suspension was filtered through a pad of Celite and the solvent was concentrated in vacuo to 1 mL. This solution was added to a second solution of 2-(4-nitrophenyl)-2-oxoacetaldehyde **7** (192 mg, 1.07 mmol) in DMF (3 mL) and stirred for 1 h at 80 °C. After cooling to RT, H<sub>2</sub>O (5 mL) was added and the obtained yellow solid was filtered, dried and gave 235 mg (78%); HPLC:  $t_R$  = 6.87 min; <sup>1</sup>H NMR (CDCl<sub>3</sub>, 500 MHz):  $\delta$  = 9.22 (s, 1H), 8.42–8.36 (m, 4H), 8.04 (d, 1H,  $J$  = 9.0 Hz), 7.48–7.45 (m, 2H), 4.02 ppm (s, 3H); <sup>13</sup>C NMR (CDCl<sub>3</sub>, 125 MHz):  $\delta$  = 161.7, 149.5, 149.0, 144.2, 143.0, 140.2, 139.5, 130.3, 128.4, 124.5, 124.4, 107.0, 56.1 ppm.

**4-(7-Methoxyquinoxalin-2-yl)aniline (17b)**: Acetic acid (1.87 mL), Fe (261 mg, 4.68 mmol) and FeCl<sub>3</sub> (127 mg, 0.78 mmol) were

added to a solution of 7-methoxy-2-(4-nitrophenyl)quinoxaline **16b** (220 mg, 0.78 mmol) in EtOH (10 mL) and stirred for 1 h at 80 °C. After cooling to RT, the solvent was removed and the residual amount was diluted in CH<sub>2</sub>Cl<sub>2</sub> and was washed with H<sub>2</sub>O. The organic layer was dried (MgSO<sub>4</sub>), filtered and the solvent was removed in vacuo. After purification by silica gel column chromatography (cyclohexane/EtOAc 1:1) 153 mg (78%) of yellow solid was obtained; HPLC:  $t_R$  = 2.43 min; <sup>1</sup>H NMR ([D<sub>6</sub>]DMSO, 500 MHz):  $\delta$  = 9.23 (s, 1H), 8.07–8.04 (m, 2H), 7.89 (d, 1H,  $J$  = 9.0 Hz), 7.36–7.32 (m, 2H), 6.73–6.70 (m, 2H), 5.72 (s, 2H), 3.95 ppm (s, 3H); <sup>13</sup>C NMR ([D<sub>6</sub>]DMSO, 125 MHz):  $\delta$  = 160.4, 151.3, 151.2, 143.3, 140.2, 136.1, 129.7, 128.5, 123.0, 120.7, 113.8, 106.7, 55.7 ppm.

**1-(5-tert-Butylisoxazol-3-yl)-3-(4-(7-methoxyquinoxalin-2-yl)phenyl)urea (18b)**: To solution of 5-tert-butylisoxazol-3-amine **10** (50 mg, 0.36 mmol) in CH<sub>2</sub>Cl<sub>2</sub> (5 mL) and triphosgene (36 mg, 0.12 mmol) was added dropwise at -10 °C a solution of Et<sub>3</sub>N (100  $\mu$ L, 0.72 mmol) in CH<sub>2</sub>Cl<sub>2</sub> (1 mL). The mixture was stirred for 1 h at this temperature. Afterward a solution of 4-(7-methoxyquinoxalin-2-yl)aniline **17b** (90 mg, 0.36 mmol) in toluene (2 mL) was added and the mixture was stirred for 2 h at 110 °C. After cooling to RT, H<sub>2</sub>O (10 mL) was added and extracted with CH<sub>2</sub>Cl<sub>2</sub> (3 × 10 mL). The solid was diluted in a small amount of DMF and heated at 100 °C. H<sub>2</sub>O (1 mL) was added and the obtained light-yellow solid was filtered to give 66 mg (44%); HPLC:  $t_R$  = 7.65 min (99%); <sup>1</sup>H NMR ([D<sub>6</sub>]DMSO, 500 MHz):  $\delta$  = 9.59 (s, 1H), 9.37 (s, 1H), 9.09 (s, 1H), 8.31–8.32 (m, 2H), 7.98 (d, 1H,  $J$  = 9.0 Hz), 7.69–7.66 (m, 2H), 7.47–7.43 (m, 2H), 6.54 (s, 1H), 3.98 (s, 3H), 1.31 ppm (s, 9H); <sup>13</sup>C NMR ([D<sub>6</sub>]DMSO, 125 MHz):  $\delta$  = 180.3, 160.6, 158.3, 151.2, 150.5, 143.2, 141.1, 140.5, 136.8, 130.1, 129.8, 128.1, 122.1, 118.5, 106.9, 92.5, 55.9, 28.3 ppm; MS (EI, 70 eV):  $m/z$  = 417 [M]<sup>+</sup>.

## Acknowledgements

The authors thank Christoph Scholz (Technische Universität Darmstadt) for help with scripting. D.B. thanks the Stiftung Industrieforschung (Essen, Germany) for support with a personal scholarship.

**Keywords:** acute myeloid leukemia · drug discovery · FMS-like tyrosine kinase 3 · inhibitors · zebrafish

- [1] a) H. J. Chung, M. R. Kamli, H. J. Lee, J. D. Ha, S. Y. Cho, J. Lee, J. Y. Kong, S. Y. Han, *Biochem. Biophys. Res. Commun.* **2014**, *445*, 561–565; b) S. Knapper, *Br. J. Haematol.* **2007**, *138*, 687–699.
- [2] M. R. Grunwald, M. J. Levis, *Int. J. Hematol.* **2013**, *97*, 683–694.
- [3] T. Kindler, D. B. Lipka, T. Fischer, *Blood* **2010**, *116*, 5089–5102.
- [4] A. D. William, A. C. Lee, S. Blanchard, A. Poulsen, E. L. Teo, H. Nagaraj, E. Tan, D. Chen, M. Williams, E. T. Sun, K. C. Goh, W. C. Ong, S. K. Goh, S. Hart, R. Jayaraman, M. K. Pasha, K. Ethirajulu, J. M. Wood, B. W. Dymock, *J. Med. Chem.* **2011**, *54*, 4638–4658.
- [5] P. Brown, D. Small, *Eur. J. Cancer* **2004**, *40*, 707–721; discussion 722–744.
- [6] S. D. Lyman, L. James, T. Vanden Bos, P. de Vries, K. Brasel, B. Gliniak, L. T. Hollingsworth, K. S. Picha, H. J. McKenna, R. R. Splett, F. A. Fletcher, E. Maraskovsky, T. Farrah, D. Foxworthe, D. E. Williams, M. P. Beckmann, *Cell* **1993**, *75*, 1157–1167.
- [7] a) D. L. Stirewalt, J. P. Radich, *Nat. Rev. Cancer* **2003**, *3*, 650–665; b) D. G. Gilliland, J. D. Griffin, *Blood* **2002**, *100*, 1532–1542.
- [8] U. Testa, *Curr. Cancer Ther. Rev.* **2013**, *9*, 181–219.
- [9] M. Nakao, S. Yokota, T. Iwai, H. Kaneko, S. Horiike, K. Kashima, Y. Sonoda, T. Fujimoto, S. Misawa, *Leukemia* **1996**, *10*, 1911–1918.

- [10] S. Mahboobi, A. Uecker, A. Sellmer, C. Cenac, H. Hocher, H. Pongratz, E. Eichhorn, H. Hufsky, A. Trumpler, M. Sicker, F. Heidel, T. Fischer, C. Stocking, S. Elz, F. D. Bohmer, S. Dove, *J. Med. Chem.* **2006**, *49*, 3101–3115.
- [11] M. Levis, J. Allebach, K. F. Tse, R. Zheng, B. R. Baldwin, B. D. Smith, S. Jones-Bolin, B. Ruggeri, C. Dionne, D. Small, *Blood* **2002**, *99*, 3885–3891.
- [12] C. C. Smith, Q. Wang, C. S. Chin, S. Salerno, L. E. Damon, M. J. Levis, A. E. Perl, K. J. Travers, S. Wang, J. P. Hunt, P. P. Zarrinkar, E. E. Schadt, A. Karsarskis, J. Kuriyan, N. P. Shah, *Nature* **2012**, *485*, 260–263.
- [13] a) N. Pemmaraju, H. Kantarjian, F. Ravandi, J. Cortes, *Cancer* **2011**, *117*, 3293–3304; b) M. Miano, C. Micalizzi, M. Calvillo, C. Dufour, *Immunol. Lett.* **2013**, *155*, 47–50; c) M. Levis, D. Small, *Int. J. Hematol.* **2005**, *82*, 100–107; d) S. Kayser, M. J. Levis, *Leuk. Lymphoma* **2014**, *55*, 243–255.
- [14] a) K. F. Tse, E. Novelli, C. I. Civin, F. D. Bohmer, D. Small, *Leukemia* **2001**, *15*, 1001–1010; b) M. Levis, K. F. Tse, B. D. Smith, E. Garrett, D. Small, *Blood* **2001**, *98*, 885–887.
- [15] a) J. Cortes, J. Foran, D. Ghirdaladze, M. P. de Vette, M. Zodelava, P. Holman, M. J. Levis, H. M. Katarjian, G. Borthakur, J. James, *Blood (ASH Annual Meeting Abstracts)* **2009**, *114*, Abstract #636; b) D. J. DeAngelo, R. M. Stone, M. L. Heaney, S. D. Nimer, R. L. Paquette, R. B. Klisovic, M. A. Caligiuri, M. R. Cooper, J. M. Lecerf, M. D. Karol, S. Sheng, N. Holford, P. T. Curtin, B. J. Druker, M. C. Heinrich, *Blood* **2006**, *108*, 3674–3681; c) W. Fiedler, R. Mesters, H. Tinnefeld, S. Loges, P. Staib, U. Duhren, M. Flasshove, O. G. Ottmann, W. Jung, F. Cavalli, R. Kuse, J. Thomalla, H. Serve, A. M. O'Farrell, M. Jacobs, N. M. Brega, P. Scigalla, D. K. Hossfeld, W. E. Berdel, *Blood* **2003**, *102*, 2763–2767; d) S. Metzelder, Y. Wang, E. Wollmer, M. Wanzel, S. Teichler, A. Chaturvedi, M. Eilers, E. Enghofer, A. Neubauer, A. Burchert, *Blood* **2009**, *113*, 6567–6571.
- [16] Q. Chao, K. G. Sprinkle, R. M. Grotzfeld, A. G. Lai, T. A. Carter, A. M. Velasco, R. N. Gunawardane, M. D. Cramer, M. F. Gardner, J. James, P. P. Zarrinkar, H. K. Patel, S. S. Bhagwat, *J. Med. Chem.* **2009**, *52*, 7808–7816.
- [17] M. McTigue, B. W. Murray, J. H. Chen, Y. L. Deng, J. Solowiej, R. S. Kania, *Proc. Natl. Acad. Sci. USA* **2012**, *109*, 18281–18289.
- [18] J. Griffith, J. Black, C. Faerman, L. Swenson, M. Wynn, F. Lu, J. Lippke, K. Saxena, *Mol. Cell* **2004**, *13*, 169–178.
- [19] K. Verstraete, G. Vandriessche, M. Januar, J. Elegheert, A. V. Shkumatov, A. Desfosses, K. Van Craenenbroeck, D. I. Svergun, I. Gutsche, B. Vergaunen, S. N. Savvides, *Blood* **2011**, *118*, 60–68.
- [20] Molecular Operating Environment (MOE), 2013.08; Chemical Computing Group Inc., 1010 Sherbooke St. West, Suite #910, Montreal, QC, H3A 2R7 (Canada).
- [21] A. Zall, D. Bensinger, B. Schmidt, *Eur. J. Org. Chem.* **2012**, 1439–1447.
- [22] D. K. Heidary, G. Huang, D. Boucher, J. Ma, C. Forster, R. Grey, J. Xu, M. Arnost, D. Choquette, G. Chen, J.-H. Zhou, Y.-M. Yao, E. D. Ball, M. Namchuk, R. J. Davies, G. Henkel, *J. Med. Chem.* **2012**, *55*, 725–734.
- [23] a) M. Giannaccini, A. Cuschieri, L. Dente, V. Raffa, *Nanomedicine* **2014**, *10*, 703–719; b) E. Lammer, G. J. Carr, K. Wendler, J. M. Rawlings, S. E. Belanger, T. Braunbeck, *Comp. Biochem. Physiol. Part C* **2009**, *149*, 196–209; c) G. Vitale, G. Gaudenzi, A. Dicitore, F. Cotelli, D. Ferone, L. Persani, *Endocr.-Relat. Cancer* **2014**, *21*, R67–83.
- [24] a) S. Deeti, S. O'Farrell, B. N. Kennedy, *J. Pharmacol. Toxicol. Methods* **2014**, *69*, 1–8; b) J. Lee, J. L. Freeman, *NeuroToxicology* **2014**, *43*, 57–64.
- [25] B.-L. He, X. Shi, C. H. Man, A. C. H. Ma, S. C. Ekker, H. C. H. Chow, C. W. E. So, W. W. L. Choi, W. Zhang, Y. Zhang, A. Y. H. Leung, *Blood* **2014**, *123*, 2518–2529.
- [26] X. Chen, M. Liu, M. K. Gilson, *Comb. Chem. High-Throughput Screen.* **2001**, *4*, 719–725.

---

Received: November 6, 2014

Revised: December 2, 2014

Published online on February 10, 2015